FULL RESEARCH ARTICLE

Development of 3D printed click-and-fit modular microfluidics for an integrated electrochemical platform

Isa Anshori[1,2] · Kurniati Laeli Munifah[1] · Eduardus Ariasena[1] · Muhammad Azhar Fa'iq[1] · Arfat Pradana[2] · Mohammad Rizki Akbar[3] · Mas Rizky Anggun Adipurna Syamsunarno[4] · Murni Handayani[5] · Agnes Purwidyantri[6] · Briliant Adhi Prabowo[7]

Abstract

In this article, we presented the development of fully modular microfluidic flow cells for an electrochemical using 3D printing. The proposed devices are potentially applied for electrochemical measurements using a small sample volume on a fully portable, reusable, fabricated, low-cost, PDMS-free, and leakage-free flow cell. This concept offers a simple, controllable sample over the conventional electrochemical platform with a three-electrode system, which requires a considerable volume of samples or a non-controllable droplet-based method for sequential protocols. We demonstrated an easy alignment and lock click-and-fit modular microfluidics, for quick and easy assembly and disassembly of flow cell modules using magnetic force instead of the screw, polymer glue, or resin. Two microfluidic modules were presented using tube- and syringe-flow cells (TFC and SFC) to integrate the screen-printed carbon electrodes in the electrochemical sensor. The proof-of-concept of the integrated sensor–microfluidic platforms was conducted under cyclic voltammetry using a tiny volume of a ferricyanide redox probe at only ~ 50 μL, differential pulse voltammetry, and square wave voltammetry. Implementing the proposed click-and-fit microfluidic modules in electrochemical detection achieves higher current peaks than droplet measurements. These flow cell modules are promising for biosensing applications using a small volume of physiological fluid samples. Our finding found that the DPV results show an enhancement sensitivity of approximately 20% using the TFC and SFC.

Keywords 3D-printed microfluidic · Flow cell · Electrochemical analysis platform · Modular

✉ Isa Anshori
isaa@staff.stei.itb.ac.id

✉ Briliant Adhi Prabowo
b.prabowo@qub.ac.uk

[1] Lab-on-Chip Laboratory, Biomedical Engineering Department, School of Electrical Engineering and Informatics, Institut Teknologi Bandung, 40132 Bandung, Indonesia

[2] Research Center for Nanosciences and Nanotechnology (RCNN), Institut Teknologi Bandung, 40132 Bandung, Indonesia

[3] Department of Cardiology and Vascular Medicine, Faculty of Medicine, Universitas Padjadjaran and Dr. Hasan Sadikin General Hospital, 40161 Bandung, Indonesia

[4] Department of Biomedical Sciences, Faculty of Medicine, Universitas Padjadjaran, 45363 Bandung, Indonesia

[5] Research Center for Nanotechnology Systems, National Research and Innovation Agency (BRIN), 15314 Tangerang Selatan, Indonesia

[6] School of Chemistry and Chemical Engineering, Queen's University Belfast, Belfast BT9 5AG, UK

[7] School of Mathematics and Physics, Queen's University Belfast, Belfast BT7 1NN, UK

1 Introduction

Microfluidic is a technology system capable of processing or manipulating liquids and gases on a scale of tens to hundreds of micrometers [1]. Microfluidic has been used for numerous applications such as biological cells encapsulation [2], fluid droplet generators [3], concentration gradient generators [4], fluid mixing and labeling on a chip [5, 6], cell and tissue culture platforms [7], and sensor integration [8, 9]. The flow cell is a platform that helps samples flow in a closed channel through the inlet–outlet channel. It is beneficial to reduce exposure to hazardous chemicals during experiments or research and to protect the sample to be analyzed [10]. Very few reagents and samples are used during the analysis with their small dimensions. Thus, it has a simple procedure to control a small volume of samples' microenvironment and increase the uniformity of sensing coverage and accuracy of a reaction [11, 12]. In addition, surface tension and capillary forces dominate the micro-workspace, making the fluid flow in a microchannel laminar [6, 13]. Flow cells have been used to deliver the sample to the sensor interface by passing through a channel that connects to the sensing chamber located inside the platform [14–16].

Although microfluidic can be applied in various fields, microfluidic platforms have limitations in their commercialization and fabrication process. Soft lithography technique is commonly used for microfluidic fabrication [17]. It has several advantages, such as enabling molecular structure control of the microfluidic platform and having high resolution of the fabrication results [18]. However, this technique requires a long process, complicated method, high cost, and often results in leakage on the platform due to a not evenly distributed pressure given during the fabrication process [19]. To overcome these problems, numerous studies have relied on micro-milling and 3D printing methods [6, 20]. This method offers a more accessible, simpler, and relatively shorter fabrication time [17]. There are several variations in 3D printing methods, such as fused deposition modeling (FDM), robocasting, multi-jet modeling (MJM), and stereolithography (SLA) [20, 21]. SLA method prints the platform layer by layer using a resin polymerized by UV light at a wavelength of about 405 nm. SLA method has a benefit in one-step fabrication than the conventional soft lithography method previously described [19]. SLA 3D printer also has the advantage of low-cost and smooth finishing printing as it firstly prints its *X–Y* design and then prints on *Z* orientation, resulting in a transparent surface.

In this study, two modular click-and-fit microfluidic platforms were fabricated using SLA 3D printing method, tube flow cell (TFC) and syringe flow cell (SFC). The permanent button-shaped magnets were applied for the simple alignment and lock of the flow cell modules, as simple as for the flow cell disassembly after the measurements. Next, the successfully printed microfluidic platforms were integrated with commercial screen-printed carbon electrodes for electrochemical sensor analysis. The platform offers better sample delivery management and uniformity of the solution during the electrochemical analysis, compared to the conventional droplet-based method. The sensor electrode was placed inside each of the microfluidic platforms and then used to test ferricyanide samples using cyclic voltammetry (CV), differential pulse voltammetry (DPV), and square wave voltammetry (SWV). In this study, we created designs to avoid leakage, eliminate external Luer tapers for fluid fitting, and make a slot to insert the SPCE into the platforms. The DPV offers the most sensitive characteristics among the voltammetry techniques because the pulse method and dual measurements can eliminate the intrinsic capacitive on the surface and the background current [22–24]. This technique can measure the very low concentration of sample down to sub-micromolar. In this article, we found that flow cell microfluidics enhance the DPV performance by up to 20%, while for CV and SWV there are insignificant changes in the measurement performance.

2 Methodology

2.1 Materials

The 3D designs of the platforms were created using Computer Aided Design (CAD) 2021 software (Autodesk® Inventor® Fusion, Autodesk Inc.) in Asus personal computer X441B (AMD Dual Core A4-9125, 4 GB 2.6 GHz). The design was then sliced using CHITUBOX 64 program (CHITUBOX™, Shenzhen, China). This slicing process made the design compatible with the Anycubic Photon Ultra 3D printer (Anycubic, Shenzhen, China). The printing material used is a resin-based Anycubic Translucent Clear UV Resin (Anycubic, Shenzhen, China). The dimensional accuracy of the fabricated channels was measured using an optical microscope from the Research Center of Nanoscience and Nanotechnology, Center for Advanced Sciences, Bandung Institute of Technology (ITB). The tools and materials used for sample testing application are 1.5 ml microtubes, 5 ml vial bottles, micropipettes, pipette tips, blower, Zimmer & Peacock (ZP) Ana Fleuve EIS potentiostat, connector cables, Zimmer & Peacock hyper-value screen-printed carbon electrodes (ZP HV-SPCE or simply SPCE), personal computer (laptop), retort stand and clamp, sulfuric acid (0.5 M H_2SO_4), various concentrations of potassium ferricyanide ($K_3[Fe(CN)_6]$) solution at 10 mM pH 7.4 phosphate buffer saline (PBS), and deionized (DI) water.

Fig. 1 The 3D designs of the click-and-fit microfluidic platforms using magnets for the modules bonding lock. **a** The upper part of tube flow cell (TFC) type; **b** the upper part of syringe flow cell (SFC) type; and **c** the bottom part for both types. The four cylindrical tubes are the magnet holders for the modules
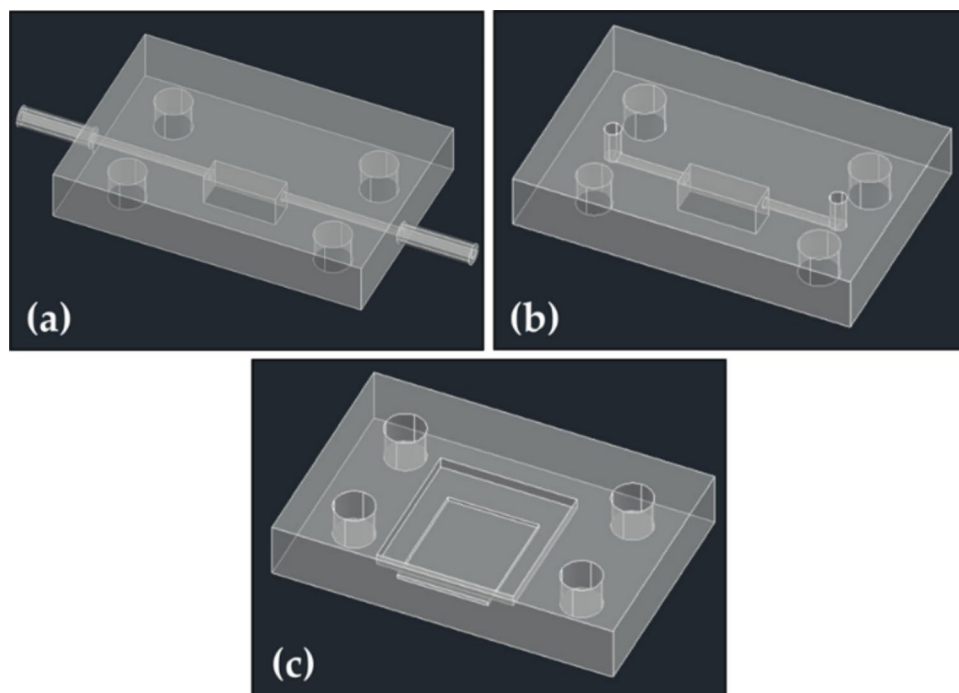
2.2 Flow cell designs

The designs of the TFC and SFC microfluidic platforms are divided into the upper and the bottom part. At the bottom part, there is a place to put a gasket with a size of 13 mm × 12 mm × 1 mm and a slot to place the inserted SPCE with a size of 10 mm × 8 mm × 0.35 mm. The SPCE full size is 25 mm × 7 mm × 0.3 mm. The channel diameter is 0.3 mm for both TFC and SFC. Meanwhile, in the upper part, there is a difference in design between the TFC and SFC. For the TFC, a closed connecting canal with the inlets and outlets is on the edge sides of the platform. While for the SFC, the inlet-outlets are in the form of cylindrical chambers placed on the top side of the platforms. Figure 1a shows the design of the upper part of the TFC type, Fig. 1b shows the design of the upper part of the SFC, and Fig. 1c shows the bottom part design of both microfluidic platform types. For the TFC type, the sample fluid is inserted using a tube from the inlet on the edge sides of the platform flowing towards the outlet. Meanwhile, the sample fluid is inserted using a syringe from the inlet on top of the platform for SFC type.

For both of the microfluidic platform types, a fundamental block with dimensions of $(30 \times 20 \times 5)$ mm^3 is formed when the upper and bottom parts of the platform are connected. The two parts of the platforms are connected using four magnets installed on each part, with each magnet's diameter and height of 3 mm. The connecting canal at the upper part of both platform types has a diameter of 0.3 mm. The chamber that connects the canal has a 25 mm × 7 mm × 0.3 mm dimension. For the TFC type, the

"integrated Luer" connected the tubes to the inlet and outlet. This integration eliminated the need for external Luer tapers of the flow cell. The Luer design has an inner and outer diameter of 1 and 3 mm, respectively. Meanwhile, for the SFC type, the cylindrical inlet–outlet on the above surface of the platform has a diameter of 0.718 mm, designed to fit the diameter of the syringe needle.

2.3 Quality control and testing

2.3.1 Qualitative fabrication results and testing

The fabrication and inspection methods were described in our previous study [20]. The channel dimension analysis of the platforms was conducted visually by observation and measurement using an optical microscope and ImageJ application. The quality testing process was performed by flowing colored water onto the platforms. The successful parameter was determined based on the ability of good water coverage on the platform when no leakage was observed.

2.3.2 Electrochemical analysis

Electrochemical analysis of the integrated electrochemical sensor electrodes (SPCE)–microfluidic platforms were conducted to analyze the performance of the sensors after the integration to the platform using ZP Ana Fleuve EIS potentiostat kit. Potassium ferricyanide ($K_3[Fe(CN)_6]$) solution at 10 mM PBS pH 7.4 was used as the sample analyte. Before the test, the SPCE was firstly activated using a 0.5 M

H_2SO_4 solution. Next, the cyclic voltammetry method was used in this activation procedure. The cyclic voltammetry parameters were sweeping potential from 0.9 to 1.5 V (initial potential from 0.9 V), step potential of 0.01 V, scan rate of 0.1 V/s, and cycle number of 3. This process was necessary for a better electrocatalytic performance of the sensor by removing organic cross-linking from carbon and to increase surface roughness and functionality [25].

Conventional sensor test scheme analysis (without microfluidic platform integration) was also conducted as a control. It was done by dropping a 50 μL sample droplet (ferricyanide solution) on the surface of the SPCE and measuring the electrochemical analysis. This droplet volume was adjusted to the sample volume that could be stored inside the microfluidic chambers, which is around 52.5 μL or equivalently about 7 mm × 2.5 mm × 3 mm. Therefore, there were three electrochemical tests, namely conventional droplet-based, TFC platform-based, and SFC platform-based tests. There were two types of electrochemical testing conducted for each test, which are the scan rate variation test using cyclic voltammetry (CV), and the sample concentration-varied test using cyclic voltammetry (CV), differential pulse voltammetry (DPV), and square wave voltammetry (SWV) method. Four tests were conducted for each sensor–platform integration.

For the scan rate variation test, CV parameters used were sweeping potential range from −0.5 to 1 V, step potential of 0.01 V, varied scan rate (25, 50, 100, 150, 200, and 250 mV/s), and 2 cycles of scanning (the 2nd cycle data were used for analysis). The measurement for each scan rate variation was conducted with 3 repetitions. The specified potassium ferricyanide solution in this test is 30 mM. The scan rate variation test aims to ensure the diffusion-controlled reaction mechanism of the sensors [26]. A linear shift of the peak redox current due to the shift of scan rate is expected to ensure this mechanism. A similar test was conducted by Geto et al., who also used screen-printed carbon electrodes and ferricyanide solution [27].

Meanwhile, for the sample concentration-varied test, CV parameters used were sweeping potential range from −0.5 to 1 V, step potential of 0.01 V, scan rate of 50 mV/s, and 2 cycles of scanning (the 2nd cycle data were used for analysis). DPV parameters used includes a potential range from −0.4 V (initial potential) to 0.6 V, step potential of 0.01 V, pulse potential of 0.2 V, pulse interval 0.02 s, and scan rate of 0.05 V/s. Lastly, the SWV parameters comprised a potential range from −0.4 V (initial potential) to 0.6 V, step potential of 0.01 V, amplitude potential of 0.005 V, and frequency of 20 Hz. The concentration of the potassium ferricyanide solution is varied into six values: 1, 2.5, 5, 10, 30, and 50 mM. The measurement for each concentration variation was conducted with 3 repetitions. The various concentration tests measure the sensor's sensitivity in each integration. A linear shift of the peak redox current due to the shift of the analyte concentration was targeted. The electrochemical analysis methods used in this testing are the
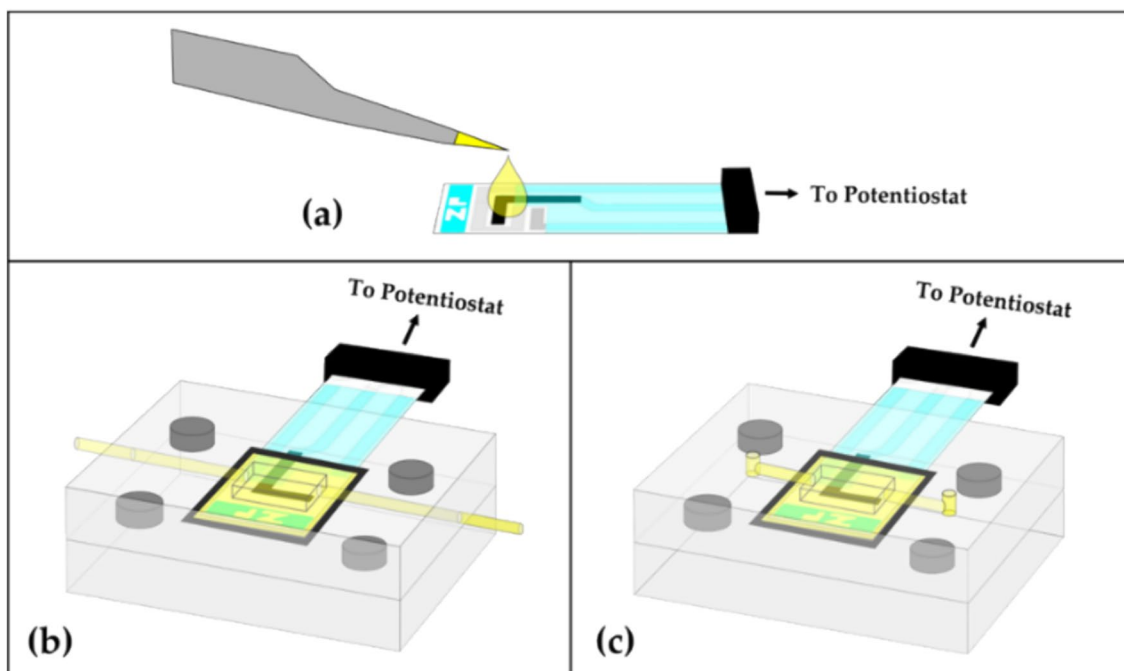

Fig. 2 The electrochemical analysis setups used in this study. **a** Conventional droplet testing setup and **b** TFC-based setup, and **c** SFC-based integration setup. The grey cylindrical structures in **b**, **c** are magnets for a simple alignment and lock of the flow cell

Scheme 1 **a** The flowchart of the methodology of the click-and-fit modular microfluidics fabrication, quality control, and the electrochemistry measurements. **b** The electrochemical measurement methodology of the integrated click-and-fit microfluidics (TFC and SFC) + electrochemical electrodes and the control which is using droplet-based method for three different voltammetry measurements (CV, SWV, and DPV)
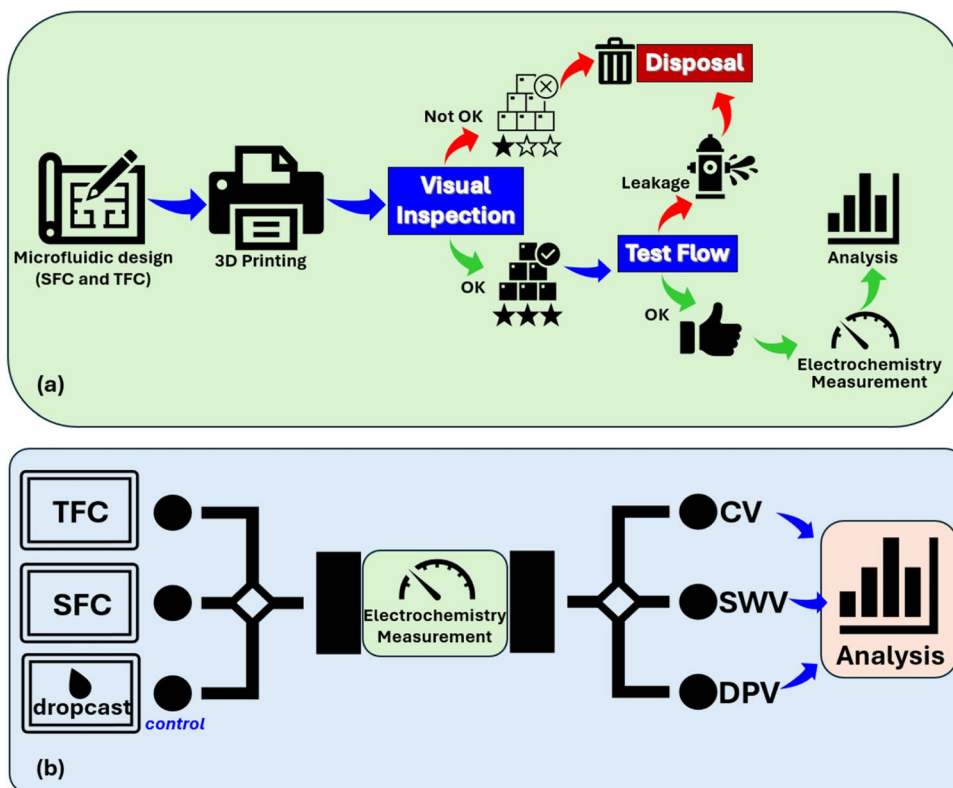

common methods usually used in electrochemical sensor studies. Several studies have used cyclic voltammetry [28, 29], differential pulse voltammetry [30, 31], and square wave voltammetry [27, 32] for electrochemical sensing tests.

Two data (using two SPCEs) were taken for each electrochemical test. First, the oxidation current peak of the voltammogram from the 2nd cycle was measured. All the data were analyzed and translated into calibration plots of the current peak value versus the corresponding square-rooted scan rate or sample concentration value. Figure 2a–c shows the

graphical electrochemical testing scheme of droplet-based, TFC-based, and SFC-based integration, respectively.

In summary, the methodology of the click-and-fit modular microfludics development can be depicted in the Scheme 1a. Meanwhile, Scheme 1b shows the flowchart of the electrochemical performance testing and analysis done in this study. The control of the test is a setup without microfluidics device, where the sample is dropped directly to the electrodes surface.

Fig. 3 The 3D printed modules of the click-and-fit flow cell. **a** The upper part of the TFC type, **b** the upper part of the SFC type, and **c** the bottom part of both microfluidics types
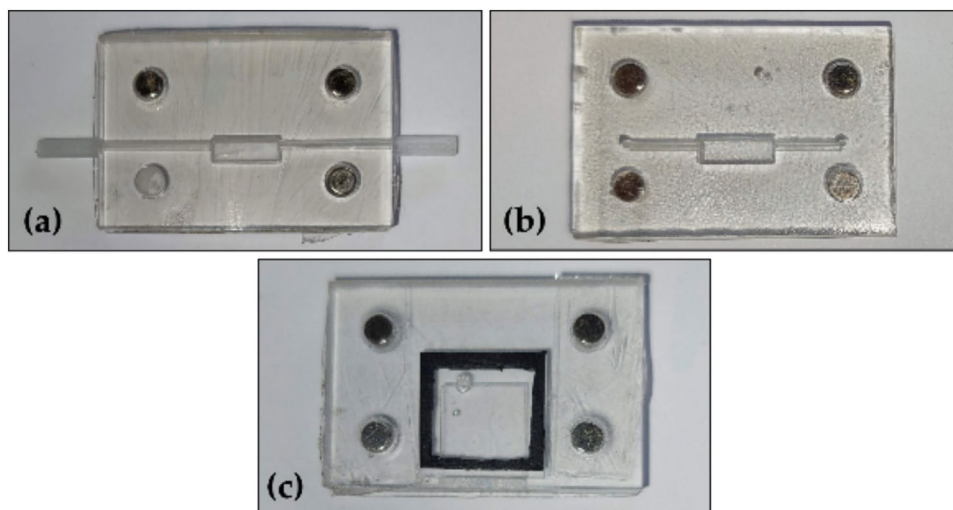
3 Results and discussion

3.1 Flow cell fabrication results and flow test

3.1.1 Fabrication results

Both platform designs were printed using a 3D printer with the following printing parameters: layer thickness of 0.05 mm, normal exposure time of 3 s, bottom exposure time of 35 s, bottom layers of 4, and off time of 1 s. The printing process took 29 min for the bottom part of both types, 29 min for the upper part of the TFC type, and 57 min for the upper part of the SFC type, with a horizontal printing orientation [20]. Specifically, for the upper part of the SFC type, since there is a hole in each side of the platform (top and bottom), 75% of support was used on one side during the printing process to prevent the platform from collapsing during the printing process. Therefore, it is necessary to smooth the platform surface of the support using a sanding sponge after printing. The clear spray could also be added to improve the visual quality of the observations so that the canals inside the platform can be seen clearly. Figure 3a shows the upper part of the TFC type platform, Fig. 3b shows the upper part of the SFC-type platform, and Fig. 3c shows the fabricated bottom part of both platform types.

The installation of the SPCE into the microfluidic platforms can be seen in S1 Fig (a and b) in the supporting information file for the TFC and SFC types, respectively. Cylindrical magnets were used as the alignment and lock, namely click-and-fit, between the upper and bottom part of the module (to form the fundamental block) inspired by LEGO [33], and a gasket was used to prevent the leakage of the platform. The platform parts were arranged in order from the lowermost section: the bottom part of the block, 8 magnets, a rectangular gasket, and the upper part of the block. Then, SPCE is inserted from the slit on the side of the platform connected to the SPCE slot.

3.1.2 Qualitative flow testing

The fluid flow testing was conducted using the liquid pump for TFC type and manually using a syringe for SFC type. The test results show that there is no leakage on the platforms. Figure 4a, b show the delivery of liquid using a tube from the left tube (inlet) to the right tube (outlet). Figure 4c, d show liquid delivery using a syringe from the top-left inlet to the top-right outlet. The liquid has fully covered the three electrodes area from the SPCE on both platforms.

## 3.2 Basic eletrochemical analysis testing results

This section shows the electrochemical analysis testing results of the integrated electrochemical sensor electrodes–microfluidic platforms. The results are shown and explained sequentially from the scan rate-varied cyclic

Fig. 4 The blue-dyed water flow on the TFC platform testing: **a** before and **b** after the flow reaches the electrode chamber; and the SFC platform: **c** before and **d** after the flow reaches the electrode chamber
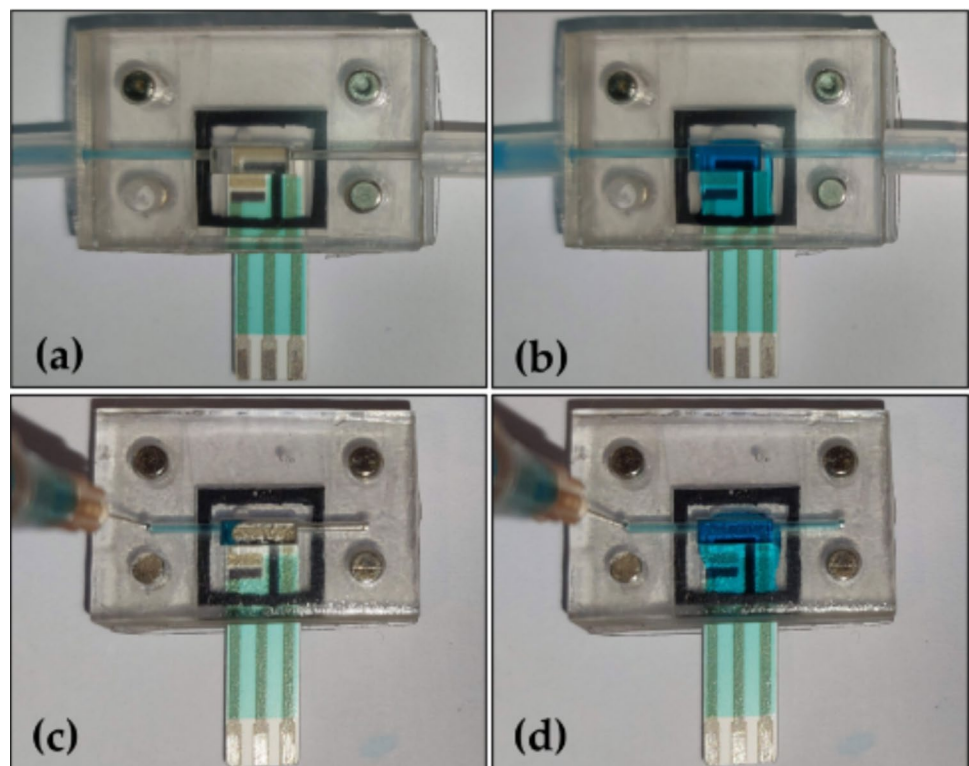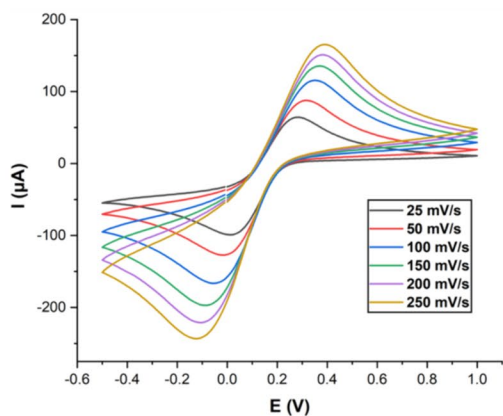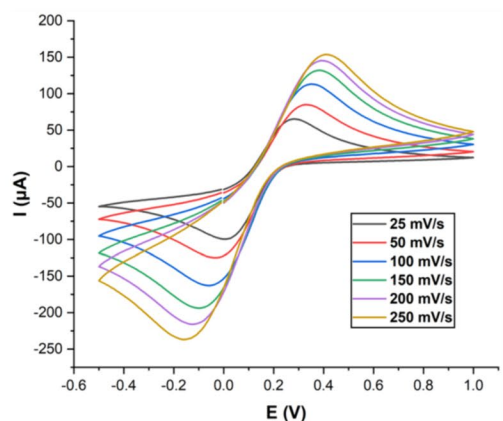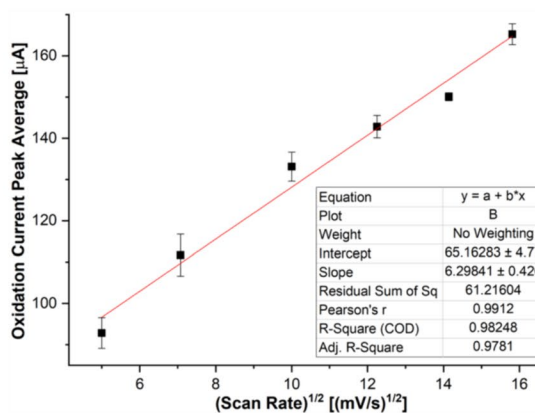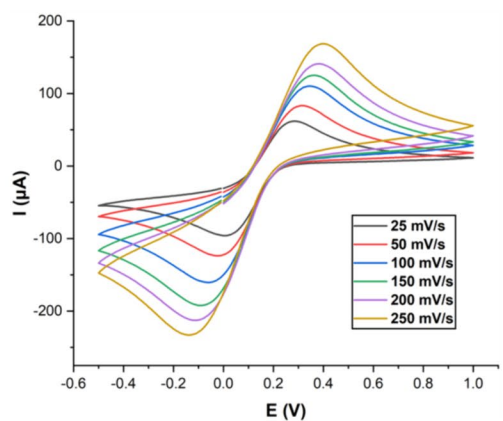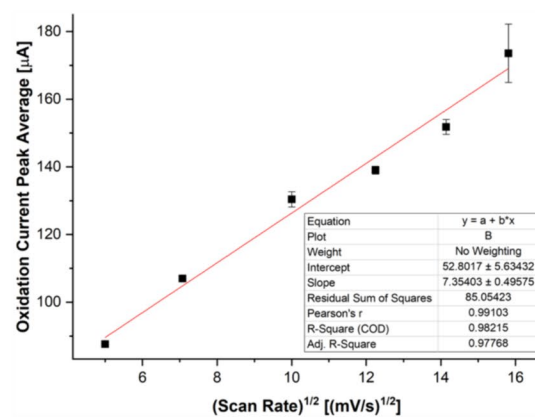
(a)
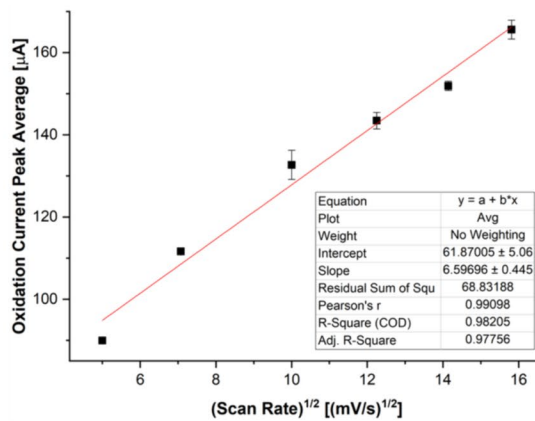
(b)

(c)

(d)

(e)

(f)

Fig. 5 Cyclic voltammetry test with various scan rates of 30 mM K$_3$[Fe(CN)$_6$] (10 mM PBS) using 50 µL droplet sample on the surface of SPCE (**a**, **b**), TFC flow cell (**c**, **d**), and SFC flow cell (**e**, **f**). **a**, **c**, **e** Cyclic voltammograms at several scan rate variations; **b**, **d**, **f** linear regression and calibrations plots of oxidation current peak average vs. square rooted potential scan rate

voltammetry test, concentration-varied cyclic voltammetry test concentration-varied differential pulse voltammetry test, and concentration-varied square wave voltammetry test.

3.2.1 Cyclic voltammetry scan rate variation

The data of the scan rate-varied cyclic voltammetry tests are shown sequentially from conventional droplet-based, TFC

platform-based, and SFC platform-based tests. Figure 5a, c, e shows the cyclic voltammograms of 30 mM $K_3[Fe (CN)_6]$ (10 mM PBS) detection at several scan rate variations of conventional droplet-based, TFC platform-based, and SFC platform-based SPCE-microfluidic platform integration schemes, respectively. The results show that an increase in redox current occurs as the value of the scan rate increases. The calibration plots in Fig. 5b, d, f shows a linear relation between square-rooted scan rate and the oxidation current peak average of potassium ferricyanide CV detection with R^2 (coefficient of determination) values of 0.9821, 0.9825, 0.9822, respectively. Based on Randles–Ševčík equation (Eq. 1), this relation indicates a diffusion-controlled reaction mechanism of the sensor increases as the scan rate enhanced [34]. This result is in a good agreement with the equation, that relation between the value of peak redox current (i_p) and the square root of scan rate (ν) used during CV analysis is proportional, as described:

$$i_p = \left(2.69 \times 10^5\right)n^{\frac{3}{2}}Ac\sqrt{\nu D} \tag{1}$$

where i_p is current peak (A), n is the amount of electrons transferred (mol), A is electrode area (cm^2), c is concentration of the solution (mol/cm^3), ν is scan rate (V/s), and D is the diffusion coefficient (cm^2/s).

3.2.2 Comparative electrochemistry measurements with various sample concentrations

The sample concentration-varied electrochemistry measurement data are shown sequentially from conventional droplet-based, TFC platform-based, and SFC platform-based tests with different concentrations of $K_3[Fe(CN)_6]$. We measured the three different configurations of the sample delivery in the electrode using cyclic voltammetry, differential pulse voltammetry, and square wave voltammetry.

Similar trends were demonstrated in the three different voltammetry schemes that the higher redox current can be achieved as the value of the sample concentration increases—the cyclic voltammetry measurement using varied sample concentrations as presented in Fig S2 and listed in Table S1 in the supporting information file. The oxidation current peak for several concentrations was compared between droplet testing (control) and TFC or SFC-based tests by calculating the percentage of current peak difference.

Similar trends for the summary of the measurement of the pulse voltammetry and square wave voltammetry are presented in Fig. 6, and Fig S3 in the supporting information file. In comparison, the data are summarized in S2 and S3 Tables, respectively, in the supporting information file. As it can be seen, there is a significant difference in the current peak average value between the conventional droplet-based

scheme and the integrated SPCE-microfluidic platform, especially for pulse voltammetry. A current enhancement value of 7.59% for TFC and 5.13% for SFC were obtained for differential pulse voltammetry (DPV). While for square wave voltammetry, the current enhancements were insignificantly different. It indicates that the CV and SWV have an identical performance in the measurements.

It also indicates that both CV and SWV have a longer time for the electrode to respond to the voltage; therefore, the uniform sample coverage using flow cells does not significantly affect the electrode response compared to the droplet measurement. In contrast, using differential pulse voltammetry, there is a concise time response of the SPCE (20 ms). In this short pulse interval, the oxidation reaction in a uniform sample coverage by flow cell plays a significant role compared to the droplet method [35]. This phenomena is because of the surface tensions in the droplet are significantly different on the surface, in the middle, and in the electrode interface [36, 37]. Therefore, the charge accumulation in the electrode interfaces was a slow response to the voltage sweep. The non-uniform surface tension effect can be reduced using the flow cell devices; therefore, the current peaks are dramatically improved in the pulse voltammetry. This can be caused by a more even interaction between the analyte sample (potassium ferricyanide) and the electrode surface in an electrochemical sensing process that uses a microfluidic platform. In droplet-based detection, the sample formed a contact angle because of the hydrophobicity of the electrode surface. An uneven sample surface was formed above the electrode surface. Meanwhile, using microfluidic platforms, the analyte sample is forced to be detained following the chamber shape of the platform. Thus, a uniform distribution of samples can be obtained on all electrode surfaces.

The summarized sensing performance through electrochemical analysis detection of our proposed integrated platforms can be seen in Table 1. The DPV measurements' sensitivity is significantly higher when using TFC and SFC. From the CV and SWV measurement performance, the TFC and SFC offer identical results. From the microfluidic configuration with the interchangeable feature of the top layer, each design offers different advantages in different pumping and observation. For example, the TFC flow cell can be beneficial in using various pumps, such as a peristaltic pump. In addition, the TCF design offers a better observation view by the user over the sample delivery and can be helpful for such experiments under an optical imaging system. On the other hand, the SFC flow cell can be beneficial if the user uses a syringe with the needle as the only option for the source of sample delivery. The observation of the sample delivery has a narrower view. This result shows another piece of evidence that by using microfluidic, all surfaces of the electrode have a consistent distribution of samples, thus
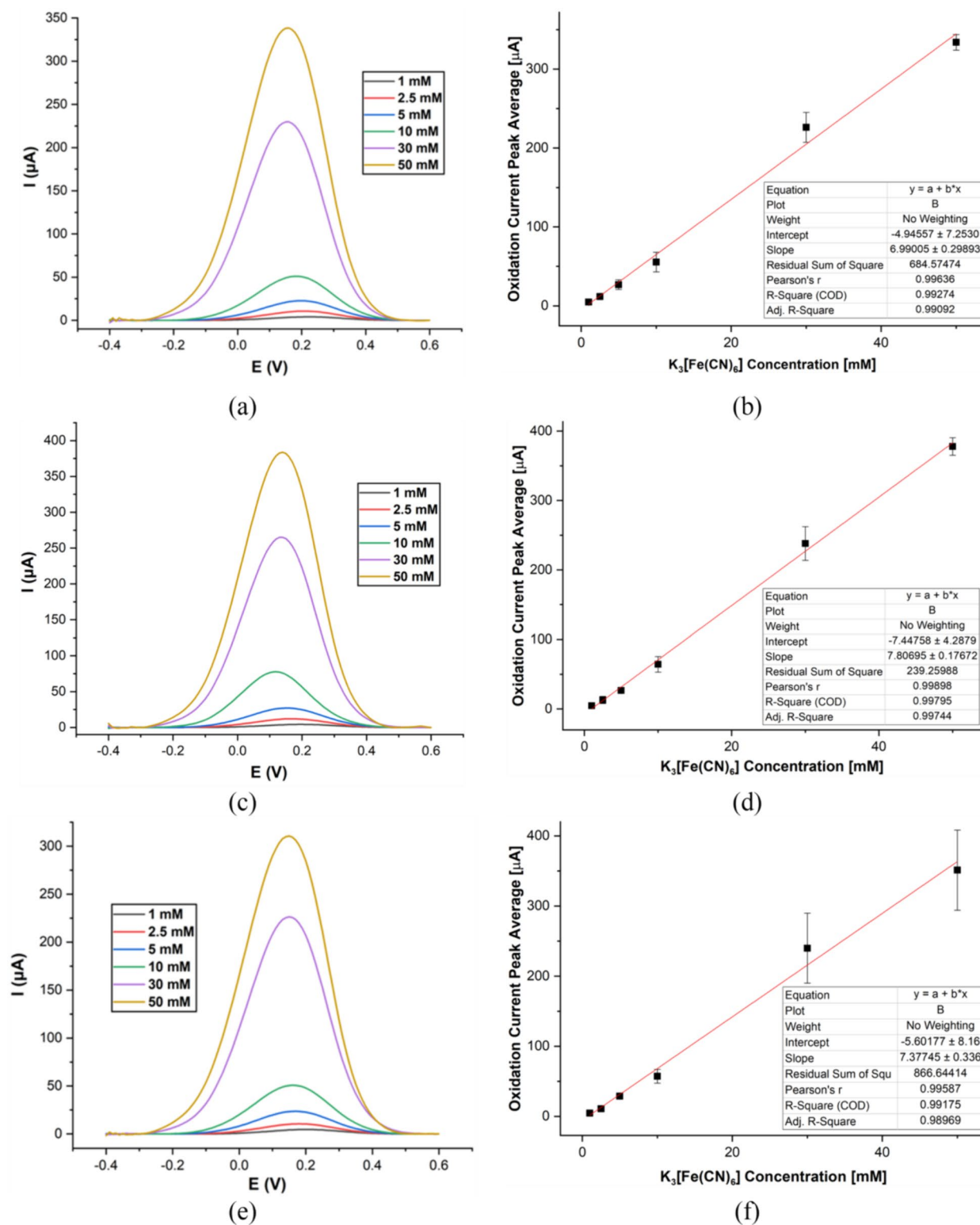
Fig. 6 Pulse voltammetry testing of $K_3[Fe(CN)_6]$ with different concentrations using 50 μL droplet sample on the surface of SPCE (**a**, **b**), TFC flow cell (**c**, **d**), and SFC flow cell (**e**, **f**). **a**, **c**, **e** Differential pulse voltammograms at several $K_3[Fe(CN)_6]$ concentrations; **b**, **d**, **f** Linear regression and calibrations plots of oxidation current peak average vs. $K_3[Fe(CN)_6]$ concentrations. The calibration plots in **b**, **d**, **f** show a linear relation between $K_3[Fe(CN)_6]$ concentration and the oxidation current peak average of the DPV detection with R^2 (coefficient of determination) values of 0.9927, 0.9980, 0.9918, respectively. The sensitivity of the detection based on the slope of the calibration plot is 6.9901 ± 0.2990, 7.8070 ± 0.1767, and 7.3775 ± 0.3360 μA/mM for droplet, TFC, and SFC scenarios, respectively

Table 1 The comparative performances of the electrochemical measurements using different methods

Electrochemical platform integration	CV		DPV		SWV	
	Sensitivity (µA/mM)	R^2	Sensitivity (µA/mM)	R^2	Sensitivity (µA/mM)	R^2
Droplet-based	3.8919 ± 0.1170	0.9964	6.9901 ± 0.2990	0.9927	0.2873 ± 0.0022	0.9998
TFC	3.8849 ± 0.0730	0.9986	7.8070 ± 0.1767	0.9980	0.3317 ± 0.0058	0.9988
SFC	3.9302 ± 0.0803	0.9983	7.3775 ± 0.3360	0.9918	0.3167 ± 0.0064	0.9984

making the working sensitivity of the electrode better. Thus, the sensitivity value is increased when using the microfluidic platform. The integrated flow cell in the electrochemistry system offers a manageable sample delivery and uniformity of the liquid on the sensor surface, compared to the droplet-based method. Indeed, the droplet-based measurement will be beneficial in terms of simplicity, straightforwardness, and cost. Due to surface tension in the small sample volume, the measurement accuracy could be less accurate. Our finding found the DPV results show an enhancement sensitivity of approximately 20% using the TFC and SFC. This finding agrees with the previous studies that DPV technique significantly eliminates the capacitive and background current by dual transition measurements during the pulse excitations [38]. Thus, the DPV voltammetry performs a highly sensitive measurement that is suitable for low-concentration samples, such as biosensors, for early detection.

4 Conclusion

The click-and-fit microfluidics flow cells have been fabricated and demonstrated for the electrochemical sensing platforms, especially for DPV method. The proposed device shows the simple assembly and disassembly modules integrated from simple alignment and locks using cylindrical magnets. The electrochemical measurements show that by using the click-and-fit flow cell modules, higher current peaks were achieved. It indicates that the proposed flow cell enhances the uniformity of sample distribution to the electrochemical electrodes. This proposed flow cell is promising for the next roadmap for biochemical sample measurement that requires a low volume of sample, real-time control flow, and low-cost and disposable flow cell. The proposed microfluidic were tested under the standard acidic sample and can be reusable for several measurements with insignificant deviations. We intend to use this integrated system for biosample, in which the sample environment is moderate. For the harsh environment sample, we believe the identical design can still be used, and we just need to replace the resin type during the 3D printing process. Several commercial resins are suitable in an acid environment due to their robustness. Finally, integrating the DPV technique and the flow cell is suitable for biosensing applications with low-concentration

biomarkers or environmental monitoring with part per billion (ppb) samples due to the sensitivity improvements it offers.

Declarations

Conflict of interest The authors have declared that no competing interests exist.

References

1. Gonzalez G, Roppolo I, Pirri CF, Chiappone A (2022) Current and emerging trends in polymeric 3D printed microfluidic devices. Addit Manuf 55:102867. https://doi.org/10.1016/j.addma.2022.102867

2. Morgan AJL, Hidalgo San Jose L, Jamieson WD et al (2016) Simple and versatile 3D printed microfluidics using fused filament fabrication. PLoS ONE 11:e0152023

3. Wang HC, Zhao MM, Wu LQ (2018) Fabrication of sandwich-like microfluidic chip with circular cross-section micro-channels. Int J Mod Phys B 32:1850288

4. Cabaleiro JM (2020) Flowrate independent 3D printed microfluidic concentration gradient generator. Chem Eng J 382:122742

5. Enders A, Siller IG, Urmann K et al (2019) 3D printed microfluidic mixers—a comparative study on mixing unit performances. Small 15:1804326

6. Prabowo BA, Fernandes E, Freitas P (2022) A pump-free microfluidic device for fast magnetic labeling of ischemic stroke biomarkers. Anal Bioanal Chem 414:2571–2583. https://doi.org/10.1007/s00216-022-03915-w

7. Yuen PK, Goral VN (2010) Low-cost rapid prototyping of flexible microfluidic devices using a desktop digital craft cutter. Lab Chip 10:384–387

8. Siller IG, Preuss J-A, Urmann K et al (2020) 3D-printed flow cells for aptamer-based impedimetric detection of *E. coli* crooks strain. Sensors 20:4421

9. Purwidyantri A, Ipatov A, Domingues T et al (2022) Programmable graphene-based microfluidic sensor for DNA detection. Sens Actuators B Chem 367:132044. https://doi.org/10.1016/j.snb.2022.132044

10. dos Santos DM, Cardoso RM, Migliorini FL et al (2022) Advances in 3D printed sensors for food analysis. TrAC Trends Anal Chem 154:116672. https://doi.org/10.1016/j.trac.2022.116672

11. Kalkal A, Kumar S, Kumar P et al (2021) Recent advances in 3D printing technologies for wearable (bio)sensors. Addit Manuf 46:102088. https://doi.org/10.1016/j.addma.2021.102088

12. Jean H, Saha T, Tey T et al (2020) Quartz crystal microbalance-based biosensors as rapid diagnostic devices for infectious diseases. Biosens Bioelectron 168:112513. https://doi.org/10.1016/j.bios.2020.112513

13. Zhou T, Yang J, Zhu D et al (2017) Hydrophilic sponges for leaf-inspired continuous pumping of liquids. Adv Sci. https://doi.org/10.1002/advs.201700028

14. Li S, Zhang C, Wang S et al (2018) Electrochemical microfluidics techniques for heavy metal ion detection. Analyst 143:4230–4246

15. Hondred JA, Johnson ZT, Claussen JC (2020) Nanoporous gold peel-and-stick biosensors created with etching inkjet maskless lithography for electrochemical pesticide monitoring with microfluidics. J Mater Chem C Mater 8:11376. https://doi.org/10.1039/d0tc01423k

16. Heidt B, Rogosic R, Leoné N et al (2021) Topographical vacuum sealing of 3d-printed multiplanar microfluidic structures. Biosensors (Basel). https://doi.org/10.3390/bios11100395

17. Gale BK, Jafek AR, Lambert CJ et al (2018) A review of current methods in microfluidic device fabrication and future commercialization prospects. Inventions 3:60. https://doi.org/10.3390/INVENTIONS3030060

18. Faustino V, Catarino SO, Lima R, Minas G (2016) Biomedical microfluidic devices by using low-cost fabrication techniques: a review. J Biomech 49:2280–2292

19. Chen C, Mehl BT, Munshi AS et al (2016) 3D-printed microfluidic devices: fabrication, advantages and limitations—a mini review. Anal Methods 8:6005–6012

20. Anshori I, Lukito V, Adhawiyah R et al (2022) Versatile and low-cost fabrication of modular lock-and-key microfluidics for integrated connector mixer using a stereolithography 3D printing. Micromachines (Basel) 13:1197. https://doi.org/10.3390/mi13081197

21. Sharafeldin M, Jones A, Rusling JF (2018) 3D-printed biosensor arrays for medical diagnostics. Micromachines (Basel) 9:1–22. https://doi.org/10.3390/mi9080394

22. Habibi B, Abazari M, Pournaghi-Azar MH (2012) A carbon nanotube modified electrode for determination of caffeine by differential pulse voltammetry. Cuihua Xuebao/Chin J Catal 33:1783–1790. https://doi.org/10.1016/s1872-2067(11)60438-5

23. Deshmukh MA, Patil HK, Bodkhe GA et al (2018) EDTA-modified PANI/SWNTs nanocomposite for differential pulse voltammetry based determination of Cu(II) ions. Sens Actuators B Chem 260:331–338. https://doi.org/10.1016/j.snb.2017.12.160

24. Venton BJ, DiScenza DJ (2020) Chapter 3—voltammetry. In: Patel B (ed) Electrochemistry for bioanalysis. Elsevier, Oxford, pp 27–50

25. Wan H, Sun Q, Li H et al (2015) Screen-printed gold electrode with gold nanoparticles modification for simultaneous electrochemical determination of lead and copper. Sens Actuators B Chem. https://doi.org/10.1016/j.snb.2014.11.127

26. Hsu CH, Gupta AK, Purwidyantri A et al (2022) Sensing Alzheimer's disease utilizing au electrode by controlling nanorestructuring. Chemosensors. https://doi.org/10.3390/chemosensors10030094

27. Geto A, Noori JS, Mortensen J et al (2019) Electrochemical determination of bentazone using simple screen-printed carbon electrodes. Environ Int 129:400–407

28. Frenzel N, Hartley J, Frisch G (2017) Voltammetric and spectroscopic study of ferrocene and hexacyanoferrate and the suitability of their redox couples as internal standards in ionic liquids. Phys Chem Chem Phys 19:28841–28852

29. Nkunu ZN, Kamau GN, Kithure JG, Muya CN (2017) Electrochemical studies of potassium ferricyanide in acetonitrile-water media (1: 1) using cyclic voltammetry method. Int J Sci Res Innov Technol 4:52–58

30. Tajik S, Orooji Y, Karimi F et al (2021) High performance of screen-printed graphite electrode modified with Ni–Mo-MOF for voltammetric determination of amaranth. J Food Meas Char 15:4617–4622

31. Faradilla P, Setiyanto H, Manurung RV, Saraswaty V (2022) Electrochemical sensor based on screen printed carbon electrode–zinc oxide nano particles/molecularly imprinted-polymer (SPCE–ZnONPs/MIP) for detection of sodium dodecyl sulfate (SDS). RSC Adv 12:743–752

32. Wang S, Huang Z, Liu M et al (2012) Application of disposable screen-printed electrode as an epirubicin sensor and relation among whole blood and tissue concentrations of epirubicin. Int J Electrochem Sci 7:1543–1555

33. Nie J, Gao Q, Qiu J et al (2018) 3D printed Lego®-like modular microfluidic devices based on capillary driving. Biofabrication 10:35001

34. Speiser B (2007) Linear sweep and cyclic voltammetry. Encycl Electrochem. https://doi.org/10.1002/9783527610426.BARD030201

35. Cheng J, Wang X, Nie T et al (2020) A novel electrochemical sensing platform for detection of dopamine based on gold nanobipyramid/multi-walled carbon nanotube hybrids. Anal Bioanal Chem 412:2433–2441. https://doi.org/10.1007/s00216-020-02455-5

36. Song M, Mehrabian N, Karuturi S, Dickey MD (2021) Jumping liquid metal droplets controlled electrochemically. Appl Phys Lett 118:81601. https://doi.org/10.1063/5.0036416

37. Yan J, Mangolini F (2021) Engineering encapsulated ionic liquids for next-generation applications. RSC Adv 11:36273–36288. https://doi.org/10.1039/d1ra05034f

38. Gupta RK (201AD) Organic electrodes. Springer, Cham